frontiers | Frontiers in Ecology and Evolution

TYPE Original Research
PUBLISHED 14 February 2023
DOI 10.3389/fevo.2023.1119869

OPEN ACCESS

EDITED BY
Kunshan Bao,
South China Normal University,
China

REVIEWED BY
Yongdong Zhang,
South China Normal University,
China
Xiaonan Zhang,
Yunnan University,
China

*CORRESPONDENCE
Can Zhang
✉ czhang@niglas.ac.cn
Haixia Zhang
✉ hxzhang@niglas.ac.cn

SPECIALTY SECTION
This article was submitted to Paleoecology, a section of the journal Frontiers in Ecology and Evolution

RECEIVED 09 December 2022
ACCEPTED 23 January 2023
PUBLISHED 14 February 2023

CITATION
Yan T, Zhang C, Zhang H, Sun X, Liu Y, Liu R, Zhang W and Zhao C (2023) Quantitative temperature and relative humidity changes recorded by the Lake Cuoqia in the southeastern Tibetan Plateau during the past 300 years.
Front. Ecol. Evol. 11:1119869.
doi: 10.3389/fevo.2023.1119869

Quantitative temperature and relative humidity changes recorded by the Lake Cuoqia in the southeastern Tibetan Plateau during the past 300 years

Tianlong Yan[1], Can Zhang[2]*, Haixia Zhang[2]*, Xiaoshuang Sun[3], Yilan Liu[2], Ruikun Liu[1], Wei Zhang[1] and Cheng Zhao[2,4]

[1]School of Geography, Liaoning Normal University, Dalian, China, [2]State Key Laboratory of Lake Science and Environment, Nanjing Institute of Geography and Limnology, Chinese Academy of Sciences, Nanjing, China, [3]School of Civil Architectural Engineering, Shandong University of Technology, Zibo, Shandong, China, [4]School of Geography and Ocean Science, Nanjing University, Nanjing, China

High-elevation lakes on the Tibetan Plateau have the advantage of sensitive response to climate changes. Multiple proxy records in lake sediments can provide a large amount of extractable information for paleoclimate reconstructions and assessing the position of recent global warming within the context of natural climate variability. In this study, we reconstruct the climatic and environmental changes over the past 300 years from a remote alpine lake (Lake Cuoqia) in the southeastern Tibetan Plateau using multiple proxies including branched glycerol dialkyl glycerol tetraethers (brGDGTs), *n*-alkanes, elements, fatty acids and their hydrogen isotopes. Due to ice-cover nature of lake surface during winter, brGDGTs mainly reflect the variation in warm-season temperature from March to October, supported by nearby instrumental data. Our reconstructed high-resolution temperature showed a continuous cooling trend between 1700 and 1950AD, followed by a rapid warming afterward, in parallel with other proxies such as *n*-alkanes and fatty acids in the same core, which is also consistent with previously published regional temperature records. The hydrogen isotope (δD) of fatty acids, similar to regional tree-ring $\delta^{18}O$, can record the history of atmospheric precipitation isotope and further indicate the variations of regional relative humidity. Our record exhibited a long-term decrease since 1700AD, in accord with the decreasing lake level inferred from the ratio of Fe/Mn. The combined pattern of reconstructed temperature and relative humidity showed consistent changes before 1950AD toward to a gradually cold-dry trend, whereas started to decouple afterward. Before 1950AD, the declined temperature and relative humidity are mainly driven by insolation and thermal contrast between the Indian-Pacific Ocean and south Asian continent. After 1950AD, decoupling of temperature and relative humidity may be related to the increased regional evaporation and human-induced emission of greenhouse gases and aerosol.

KEYWORDS

quantitative temperature, relative humidity, brGDGTs, hydrogen isotopes, past 300 years

Introduction

The southeastern Tibetan Plateau is the source of many large rivers in Asia, which is crucial to the atmospheric circulation and hydrological cycle from the regional to global scale (Ding, 1992). The meteorological data since 1950 AD showed that the heating rate of the Tibetan Plateau is twice the global average and relative humidity shows a downward trend (Chen et al., 2015). However, the

scarcity of meteorological stations and the lack of paleoclimate records limit us to perceive the mechanism of long-term climate changes (Yao et al., 2019). Thus, in order to obtain the pattern of long-term climate change, proxy-based climate researches are necessary. Moreover, this region is a refuge for many animals and plants with high biodiversity (Tan et al., 2018). Climate change in this region has an important impact on the socio-economic development and ecosystem of Southwest China. The past 300 years has been an important period for understanding the transition from nature-led to human-induced environmental changes, as well as for understanding the interaction between humans and nature. Understanding the characteristics and mechanisms of temperature and humidity changes over the past 300 years in the southeastern Tibetan Plateau is very important for assessing the climate change trend in the future.

Lake sediments have the advantages of good continuity, high resolution, climate sensitivity and large amount of extractable information. They have irreplaceable advantages in reconstructing climatic and environmental changes (Shen et al., 2010). In recent years, many records of quantitative temperature and precipitation/relative humidity have been reconstructed based on lake sediments in southeastern Tibetan Plateau (An et al., 2014; Liu X. et al., 2014; Zhang et al., 2017, 2022; Tan et al., 2018; Feng et al., 2019; Xu et al., 2019; Sun et al., 2021; Zhao et al., 2021a). Quantitative temperature reconstruction can not only understand the trend of temperature change in a long-time scale, but also obtain the absolute value and change amplitude of temperature more clearly. It is of great significance for providing more accurate future climate prediction (Kaufman et al., 2004). In addition, the reconstruction of relative humidity can increase the understanding of hydroclimatic changes in the southeastern Tibetan Plateau.

Glycerol dialkyl glycerol tetraethers (GDGTs) are a kind of membrane-spanning lipids with two C_{28} alkyl chains, 4–6 methyl substituents and 0–2 cyclopentyl moieties from bacteria and archaea (Sinninghe Damste et al., 2009; Schouten et al., 2013), which are common in lakes (Sun et al., 2011; Russell et al., 2018; Zhao et al., 2021a). Previous studies have shown that the bacterial-sourced branched GDGTs (brGDGTs) responses to temperature changes *via* producing more/less methyl branches to adjust to colder/warmer conditions (Peterse et al., 2011; Schouten et al., 2013). With the development of chromatographic separation, previous study successfully separated 5- and 6- methyl brGDGTs, further improving the reliability of temperature reconstructions (De Jonge et al., 2014). Hydrogen isotopes of fatty acids is a proxy which can well record the isotopic changes of atmospheric precipitation (Eglinton and Eglinton, 2008; Sachse et al., 2012). At present, there are few studies on precipitation/relative humidity reconstruction using hydrogen isotopes of fatty acids in southwestern China. In this study, we use multiple proxies to (1) quantitatively reconstruct temperature changes and precipitation/relative humidity over the past 300 years including brGDGTs, hydrogen isotope (δD), *n*-alkane, fatty acids and element, and (2) assess combined pattern of temperature and precipitation/relative humidity and the possible driving mechanisms.

Materials and methods

Study site

Lake Cuoqia is located in Hengduan Mountains in the southeastern Tibetan Plateau, ~20 km southwest of Shangri La County, Diqing Autonomous Prefecture, Yunnan Province (27°24′18.72″ N, 99°46′19.87″ E; elevation: 3960 m; Figure 1A). Hengduan Mountain is an important geographical boundary between the first and second steps of China, with obvious vertical zonality and dramatic changes in geomorphology and climate. Marine glaciers are developed in this area, and many glacial lakes are developed between 3,900 and 4,000 m above sea level (Zhang et al., 2012). Lake Cuoqia is lower than the forest line, with an area of 0.07 km^2, an average depth of 13.2 m and a maximum depth of 26 m (Figure 1B, Chai et al., 2018). The lake is hydrologically closed with no visible surface inflow and outflow. It is mainly supplied by atmospheric precipitation and ground melting snow water (Zhang et al., 2022). The vegetation around the lake is almost undisturbed by human activities, mainly subalpine low temperature coniferous trees, such as *Abies* and *Rhododendron* shrubs (Xiao et al., 2014).

The region is mainly affected by the Indian monsoon, with the same period of rain and heat. The region belongs to the temperate continental monsoon climate, with abundant solar radiation throughout the year and small annual temperature difference. According to the modern meteorological data of Shangri La Meteorological Station (27°30′0″ N, 99°25′12″ E; elevation: 3276.7 m), the nearest meteorological station to Lake Cuoqia, mean annual air temperature is 6.01°C, and mean annual precipitation is 624.72 mm. The temperature in this area is the highest in July (average monthly temperature 13.9°C) and the lowest in January (average monthly temperature - 2.3°C). The precipitation is mainly concentrated in June to September (Figure 1C). The monthly average humidity changes are between 58% (December) and 79% (August). From 1958 to 2015 AD, the mean annual precipitation has no obvious change, while the mean annual air temperature shows an obvious upward trend with 0.03°C/year (Figure 1D).

Sample collection and age control

In May 2014, a pair of sediment core (CQ1 and CQ2) were obtained using Hon Kajak large-diameter (9 cm) gravity sampler in the center of the Lake Cuoqia (Figure 1B). The two cores are 37 cm and 30 cm, respectively, and composed of humus black mud. The cores were sampled at an interval of 0.5 cm in the field. The samples were stored in self-sealing bags and refrigerated at 4°C for analysis. We also collected plant samples from trees, shrubs, grasses and surface soil around the lake.

CQ1 is used for proxy analysis of brGDGTs, fatty acids and its hydrogen isotopes, *n*-alkanes, total organic carbon (TOC), total nitrogen (TN) (Chai et al., 2018) and elements. CQ2 is used for $^{210}Pb/^{137}Cs$ dating to further calibrate the age model based on the CRS (Constant Rate of ^{210}Pb Supply) model (Appleby and Oldfeld, 1978). The depth-age sequence of both cores was previously published in Chai et al. (2018) and Zhang et al. (2022).

Biomarkers proxy analysis

About 1–3 g freeze-dried samples were extracted 4 times through ultrasonic shaker using organic solvents (dichloromethane: methanol = 9:1, v/v), ensuring complete extraction of organic matter from samples. After drying with N_2 gas, extracted total lipids were hydrolyzed using 6% KOH in Methyl alcohol solution for 12 h. Then, the supernatant was obtained after adding NaCl and *n*-hexane and

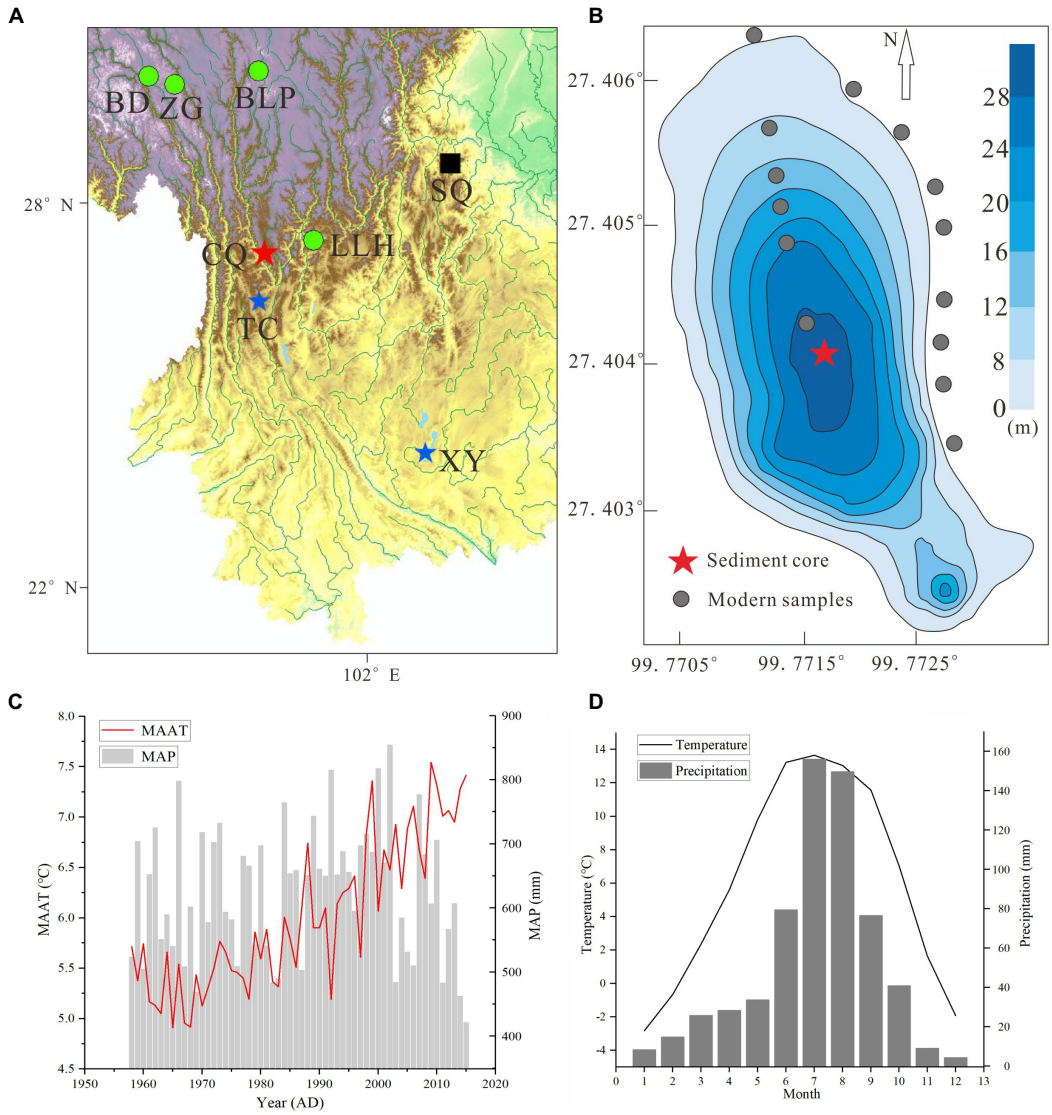

FIGURE 1
Location map and core sampling. **(A)** The map showing location of the Lake Cuoqia (CQ, red asterisks) and other paleoclimate records mentioned in this study. Blue asterisks are paleotemperature record from lakes [TC: Lake Tiancai (Zhang et al., 2017; Feng et al., 2019); XY: Lake Xingyun (Wu et al., 2018)]. Black block is stalagmite record from Shenqi cave (Tan et al., 2018). Green circle is tree ring records. [LLH: Larix trees in the low-latitude highlands (Xu et al., 2019); BLP: Batang-Litang Plateau (An et al., 2014); BD, ZG: Bangda and Zuogong (Duan and Zhang, 2014)]. **(B)** Bathymetry of the Lake Cuoqia and locations of the sediment cores (asterisks), surface sediment samples and soil samples on the catchment (grey dots). **(C)** The temperature and precipitation changes from Shangri La Meteorological Station during 1958–2015years. **(D)** Mean monthly temperature and precipitation at the Shangri-la Meteorological Station, Yunnan Province, China (data retrieved from the Meteorological Administration of China, http://data.cma.cn/). (For interpretation of the references to color in this figure legend, the reader is referred to the web version of this article).

centrifuging. Add 1.5 mL HCl (6 Mol) and 1.5 mL *n*-hexane to the bottle containing the sample solution to obtain the component of fatty acids. Finally, the neutral supernatant containing *n*-alkanes and GDGTs were further extracted through silica gel column chromatography using *n*-hexane and MeOH, respectively.

A total of 30 samples are determined for the fatty acids and δD values using Delta-V isotope ratio mass spectrometry (IRMS) instrument (Thermo Finnigan) *via* a high-temperature pyrolysis reactor at 1430°C. The instrument parameter settings and data analysis methods were referred to Liu and Liu, 2019. A total of 52 samples are analyzed for the *n*-alkanes *via* an Agilent 7,890 Gas Chromatography and the conditions for the Gas Chromatography following the previous research (Zhang et al., 2019).

A total of 68 samples are analyzed for the brGDGTs *via* UPLC-APCI-MS (the ACQUITY I-Class plus/Xevo TQ-S system) equipped with two coupled UPLC silica columns (BEH HILIC columns, 3.0 × 150 mm, 1.7 μm; Waters) in series, fitted with a pre-column and maintained at 30°C. The instrument can fully separate of 5- and 6-methyl isomers with improved chromatographic procedure. The samples were dissolved in 1000 μL *n*-hexane and injected for 4 μL for analysis. BrGDGTs were eluted at a constant flow rate of 0.4 mL/min for 80 min. The mobile phases of A and B, where A = hexane and B = hexane: isopropanol (9:1, v/v), were run isocratic ally with 82% A and 18% B for 25 min, followed by a linear gradient to 65% A and 35% B for 25–50 min, then to 100% B for 50–60 min with another 20 min re-equilibration. BrGDGTs were ionized in the APCI source at a probe temperature of

550°C, voltage corona of 5.0 μV, voltage cone of 110 V, gas flow desolvation of 1,000 L/h, gas flow cone of 150 L/h and collision gas flow of 0.15 mL/min. BrGDGTs isomers were detected using the selective ion monitoring (SIM) mode *via* $[M+H]^+$ ions at m/z 744 for the C_{46} standard, m/z 1,050, 1,048, 1,046, 1,036, 1,034, 1,032, 1,022, 1,020, and 1,018 for brGDGTs compounds (Hopmans et al., 2016). The modern samples were analyzed with the C_{46} standard and the relative concentrations of brGDGTs were calculated according to the integrated peak areas. Lipid preparation, *n*-alkanes and brGDGTs analysis were performed at the State Key Laboratory of Lake Science and Environment, Nanjing Institute of Geography and Limnology, Chinese Academy of Science. The fatty acids and its hydrogen isotopes were analyzed at State Key Laboratory of Loess and Quaternary Geology, Institute of Earth Environment, Chinese Academy of Sciences.

Parameters of average chain length (ACL) associated with *n*-alkanes and fatty acids were calculated as follow, respectively (Ficken et al., 2000; Liu and Liu, 2019).

$$\mathrm{ACL}_{n-\mathrm{alkanes}} = \begin{pmatrix} 21\times C_{21} + 23\times C_{23} \\ +\ldots+ 33\times C_{33} \end{pmatrix} / \begin{pmatrix} C_{21} + C_{23} \\ +\ldots+ C_{33} \end{pmatrix} \quad (1)$$

$$\mathrm{ACL}_{\mathrm{fatty\ acids}} = \begin{pmatrix} 20\times C_{20} + 22\times C_{22} \\ +\ldots+ 30\times C_{30} \end{pmatrix} / \begin{pmatrix} C_{20} + C_{22} \\ +\ldots+ C_{30} \end{pmatrix} \quad (2)$$

Where the C*i* is the abundance of the *i*th *n*-alkanes and fatty acids.

Reconstructions of quantitative temperature and relative humidity

The site-specific calibration of Lake Cuoqia was established using a stepwise regression method between brGDGTs fractional abundance of short-core CQ1 and the instrumental temperature record during the warm season (from March to October, $T_{M\text{-}O}$; Zhang et al., 2022). Such calibration has also been verified by reconstructed temperature record of another pair core (CQ2) since 1950 AD. Thus, the equation was further used to quantitatively reconstruct the temperature sequences of both cores over the past 300 years.

$$\begin{aligned} T_{M-O} = {} & 4.29 - 0.57\times f(IIIa) + 24.38\times f(IIa) \\ & - 3.44\times f(IIb) - 28.84\times f(Ia) \\ & - 34.19\times f(Ib) \begin{pmatrix} R^2 = 0.89, \\ RMSE = 0.24°\mathrm{C}, \\ n = 22 \end{pmatrix} \end{aligned} \quad (3)$$

Methanol correction formula is as follow (Yang and Huang, 2003):

$$\delta D_{n-\mathrm{Fas}} = \left[(2n+2)\,\delta D_{n-\mathrm{FAMEs}} - 3\delta D_{\mathrm{methanol}}\right] / (2n-1) \quad (4)$$

$\delta D_{n-\mathrm{Fas}}$, $\delta D_{n-\mathrm{FAMEs}}$ and $\delta D_{\mathrm{methanol}}$ represent value of fatty acids, fatty acid methyl ester and methanol δD, respectively. The value of $\delta D_{\mathrm{methanol}} = -123‰$.

For better discuss the driving mechanisms of climatic change, we calculated the temperature difference obtained by subtracting the average temperature of the Indian-Pacific Ocean from our reconstructed temperature. The specific method is firstly to normalize the difference between our reconstructed temperature and the temperature of the Indian-Pacific Ocean before interpolating to the same resolution.

Results

Our modern results show that the *n*-alkanes in lake surface sediments are mainly composed of long chains of C_{29} and C_{31} (Supplementary Figure S1). This is consistent with carbon chain distribution of catchment terrestrial plants (trees and shrubs) and top soils, but different from those of herbaceous plants dominated by medium chains (C_{27}) in the basin, indicating that the *n*-alkanes in the sediments of Lake Cuoqia are mainly derived from exogenous terrestrial arbors. The carbon chain distribution pattern of fatty acids showed that C_{16} and C_{22} were the main fraction in all periods (Supplementary Figure S2). C_{22} of fatty acids was applied for δD analysis due to the unclear source of C_{16} from microorganisms or terrestrial plants (Hou et al., 2006).

The reconstructed temperature shows consistent in two cores from Lake Cuoqia, showing a decline trend before 1950 AD and an increase after 1950 AD (Figure 2A). ACL values of *n*-alkanes and fatty acids changed almost same before 1930 AD, showing a continuous downward trend. After 1930, although ACL of both *n*-alkanes and fatty acids showed an upward trend, the growth rate of fatty acids was more obvious (Figure 2C). The ACL values of *n*-alkanes and fatty acids were consistent with the temperature results, both showing a change pattern of first falling and then rising. In addition, the change pattern of TOC and TN are also consistent with the temperature (Figure 2D). The δD of C_{22} from fatty acids showed a continuous decline pattern in the past 300 years (Figure 2E). The change pattern is consistent with the values of Fe/Mn (Figure 2F). The Rb/Sr. increased continuously before 1980 AD and began to decrease after 1980 AD (Figure 2G).

Discussion

Quantitative temperature reconstruction at Lake Cuoqia since 1700AD

Previous study shows that the brGDGTs in Lake Cuoqia mainly come from autochthonous sources, which are supported by multiple lines of evidence including comparison of brGDGTs distribution between surface sediments and down-core samples, ternary plots analysis (tetra-, penta-, and hexamethylated brGDGTs), relationship between the concentration of brGDGTs in surface sediments and water depth and ∑IIIa/∑IIa calculation (Zhang et al., 2022). The brGDGTs can well capture the temperature changes during the instrumental period at Lake Cuoqia with high correlation ($R^2 = 0.89$) to nearby meteorological data (Zhang et al., 2022). Using the same correction equation, we further quantitatively reconstructed the temperature changes in the past 300 years. The reconstructed temperature dropped continuously before 1950 AD and rose rapidly afterwards (Figure 2A). BIT (Branched Isoprenoid Tetraether index) values are the ratio of branched GDGTs to all fractional abundance of GDGTs (including branched and isoprenoid tetraether) and have been widely used as a proxy to evaluate the stability of the sedimentary environment (Zhang et al., 2019, 2022; Yan et al., 2021; Zhao et al., 2021a). The change of the BIT values was quite stable varying from 0.95 to 1 (Figure 2B), indicating

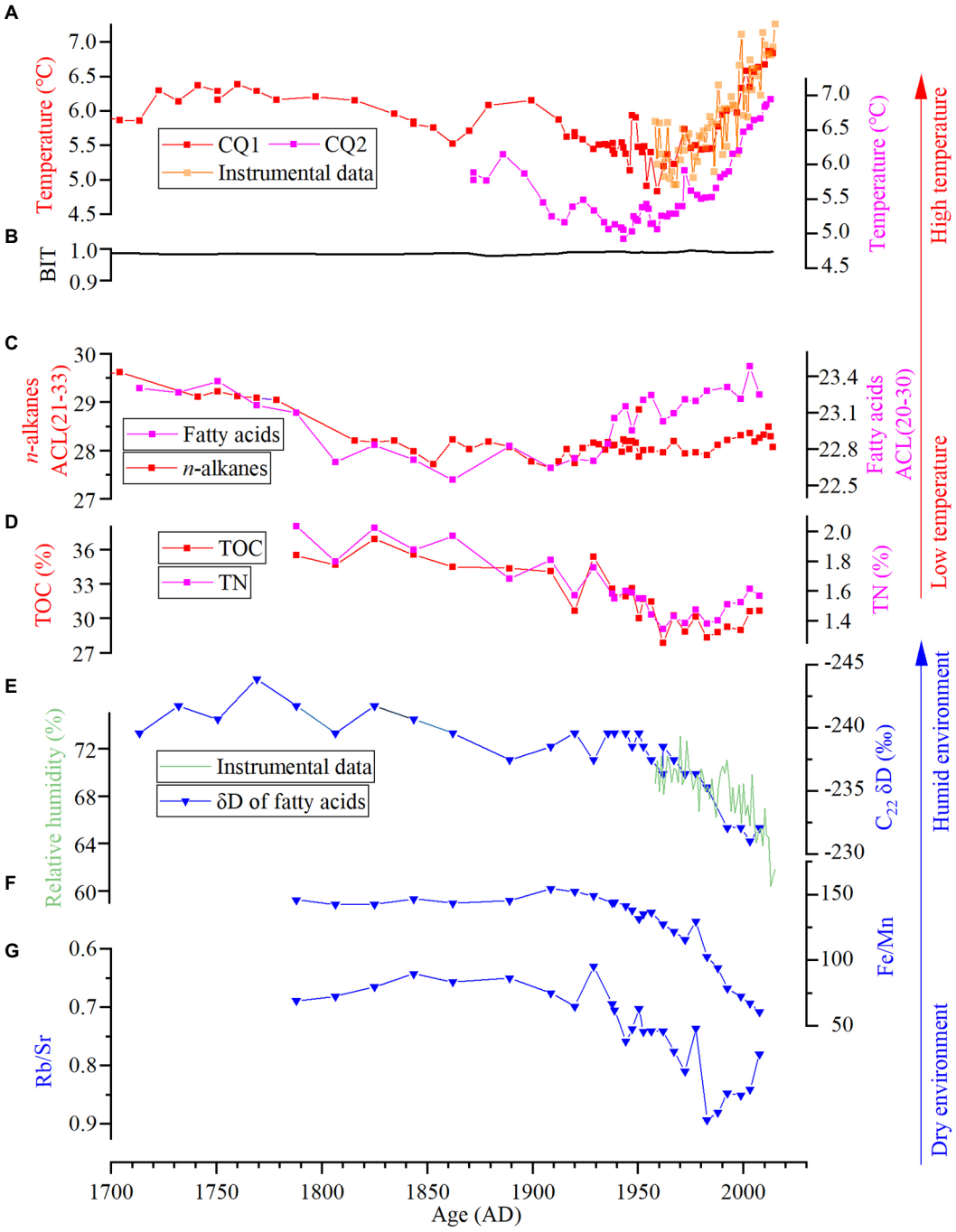

FIGURE 2
Results of multiple proxies from Lake Cuoqia. **(A)** The reconstructed temperature using brGDGTs from core CQ1 (red line) and CQ2 (magenta line). The orange line represents the warm season temperature (3–10month) from Shangri La Meteorological Station. Elevation correlation was made using a lapse rate of ~0.53°C/100m (He and Wang, 2020). **(B)** BIT values. **(C)** ACL values of fatty acids and *n*-alkanes. **(D)** TOC and TN (Chai et al., 2018). **(E)** δD of fatty acids (C_{22}, blue line) and relative humidity (green line) from instrumental data. **(F)** Fe/Mn ratio. **(G)** Rb/Sr. ratio. (For interpretation of the references to color in this figure legend, the reader is referred to the web version of this article).

stable sedimentary environment and the applicability of the calibration to the whole core. Our temperature results are supported by warm-season temperature (from March to October) from regional meteorological station data during 1958–2015 AD for both long-term trend and amplitude of variation (Figure 2A).

The reconstructed temperature shows consistent with other proxies from the same core such as ACL values of both *n*-alkanes and fatty acids, TOC and TN (Figures 2C, D). Previous study shows that the mid- and long-chains of leaf wax mainly from terrestrial plants, which is sensitive to temperature changes and can be used as an indicator of temperature changes (Zhou et al., 2005). Although the overall pattern of temperature changes is consistent, the slight discrepancy between them is possibly due to different responses to climate change. TOC and TN are two fundamental proxies for describing organic matter content in sediments, mainly reflecting the primary production of biomass which is related with regional climate changes (Meyers and Ishiwatari, 1993). The decline

of TOC and TN may indicate the gradually cold-dry climate conditions, in accord with the variation of our reconstructed temperature.

Our reconstructed temperature is also consistent with previously limited regional temperature records (Duan and Zhang, 2014; Zhang et al., 2017; Wu et al., 2018). For instance, July temperature based on subfossil chironomids from Lake Tiancai showed an overall decrease with a rapid increase after 1970 AD, albeit with an abnormal value at 1950 AD and quite low resolution (Figure 3B; Zhang et al., 2017). Our absolute temperature has lower values than Lake Tiancai for the past 300 years, which can attribute to differences of reconstructed season and elevation (higher ~60 m). Moreover, the similar long-term trend can also be observed from pollen-based July temperature record at the Lake Xingyun (Figure 3C; Wu et al., 2018). The higher-resolution warm-season (from April to September) temperature from tree ring showed a slight decrease trend before 1920 AD with a reverse afterwards (Figure 3D; Duan and Zhang, 2014). The low temperatures centered at 1870 AD and 1980 AD corresponded with our reconstructed temperature (Figure 3D). The mismatch in the warming time may be attributed to dating uncertainty. It is worth noting that our temperature shows obvious discrepancy with the trend of mean annual air temperature reconstructed by brGDGTs from Lake Tiancai and sea surface temperature from Indian-Pacific Ocean (Tierney et al., 2015; Feng et al., 2019), both showing a continuous warming (Figures 3E, F). This may be attributed to seasonal difference between warm-season and mean annual temperature, which is confirmed to be present at longer Holocene scales (Sun et al., 2021; Zhang et al., 2022). In conclusion, our reconstructed 300 years quantitative temperature is reliable and agrees well with regional limited temperature records.

Relative humidity changes over the past 300 years

Previous studies suggest that the hydrogen isotopes of fatty acids and *n*-alkanes from terrestrial plants can well record the isotopic changes of atmospheric precipitation (Eglinton and Eglinton, 2008; Sachse et al., 2012). δD of C_{22} from fatty acids has similar fraction process of *n*-alkanes δD from precipitation isotope in hydrological cycles (Hou et al., 2006; Contreras-Rosales et al., 2014). However, the controlled factors of leaf wax δD include local rainfall, soil evaporation, vegetation fractionations, etc. (Dansgaard, 1964; Cai et al., 2012; Sachse et al., 2012; Zhang et al., 2020). The water required for plants in the lake catchment mainly derived from soil water which is influenced by monsoon precipitation and soil evaporation effect (Sachse et al., 2004, 2012; Zhao et al., 2021b). Thus, leaf wax δD should mainly reflect the variations in the relative humidity. The isotopic fractionations may also exist during lipid biosynthesis in plant, and possible evapotranspiration between soil and lipid leaf wax water (Sachse et al., 2012). Some studies from southwestern China demonstrate that the isotope (δD and $\delta^{18}O$) of tree ring indeed indicates the changes of relative humidity on centennial time scale (An et al., 2014), and has been verified by the regional instrumental data. Note that the effect of vegetation fractionation also exists in tree-ring δD with little influence, similar to our leaf wax δD of fatty acid (An et al., 2014). Therefore, our isotope records the changes of regional relative humidity with positive δD of C_{22} indicating dry environment, and vice versa.

In the past 300 years, the gradually enriched δD of C_{22} from the Lake Cuoqia indicates a continuously dry condition, which shows good relation with the relative humidity measured by instrument data over the past decades (Figure 2E). Our δD-based relative humidity is also consistent with the ratio of Fe/Mn from the same core (Figure 4B). Fe/Mn can indicate redox state and further indicate the rise and fall of lake level with high ratio of Fe/Mn corresponding to high lake level, and vice versa (Mackereth, 1966). Similar changes can also be observed in another proxy of Rb/Sr. ratio in the same core (Figure 2G), which is widely used to reflect the intensity of chemical weathering with low values for intense chemical weathering related to humid environment, and vice versa (Chen et al., 2008; Liu J. et al., 2014).

The consistent changes of the relative humidity can also be recorded by other geological archives including tree ring, stalagmite and lake (An et al., 2014; Xiao et al., 2014; Tan et al., 2018; Xu et al., 2018, 2019). For example, the relative humidity, reconstructed by high-resolution tree ring $\delta^{18}O$ from Batang-Litang Plateau (BLP) of southeastern Tibetan Plateau (Figure 1A), showed a long-term drying trend in the past 300 years (Figure 4C; An et al., 2014). Also, similar trend can be observed in another $\delta^{18}O$ of tree ring from low-latitude highlands (LLH) of southwestern China (Figure 1A), revealing an apparent drying trend especially after 1840 AD (Figure 4D; Xu et al., 2018, 2019), which can be supported by the reconstructed cloud cover records using composite $\delta^{18}O$ of three tree-ring chronologies from southeastern Tibetan Plateau (Figure 4E; Liu X. et al., 2014). Similarly, many $\delta^{18}O$ records of stalagmite in nearby regions also show consistent changes with our reconstructed relatively humidity. For instance, the precipitation index and $\delta^{18}O$ of stalagmite from Shenqi Cave (SQ) in southwestern China (Figures 4F, G; Tan et al., 2018) showed a persistent positive trend, indicating a drying environment. In addition, the gradually drying environment is also supported by pollen data in sediments of Lake Tiancai, in which the tree pollen of *Tsuga* gradually decreases (Xiao et al., 2014). In summary, the reconstructed relative humidity is consistent with proxies from same core and is supported by instrumental data and regional precipitation/relative humidity records.

Combined pattern of temperature and relative humidity and driving mechanisms

Our reconstructed temperature and relative humidity showed consistent changes between 1700 AD and 1950 AD toward to gradually cold-dry trend, whereas started to decouple after 1950 AD, manifested as increasing temperature and decreasing relative humidity (Figures 2A,E). The combined pattern of reconstructed temperature and relative humidity is characterized with decoupling at 1950 AD, when the reason has not yet completely recorded and discussed by regional archives. Here, we focus on analyzing and explaining the underlying causes and driving factors of decoupling before and after 1950 AD.

The continuous decrease of temperature and relative humidity before 1950 AD was in accord with the decreasing warm-season insolation (from March to October) at 26° N (Figure 3H; Laskar et al., 2004; Sun et al., 2021). The decreasing insolation reduced total energy received at the earth surface, resulting into the decline in regional temperature. The decreasing insolation also weakened the intensity of Indian summer monsoon and further reduced the precipitation and/or relative humidity in our study area (Tan et al., 2018). Moreover, the persistent decline of relative humidity may be related to the decreasing thermal contrast between sea surface temperatures of the tropical Indian-Pacific Ocean and land temperature in our region (Figure 3G), which determines the intensity of water-vapor transports dominated by the Indian summer monsoon (Bansod et al., 2003; Feng and Hu, 2005;

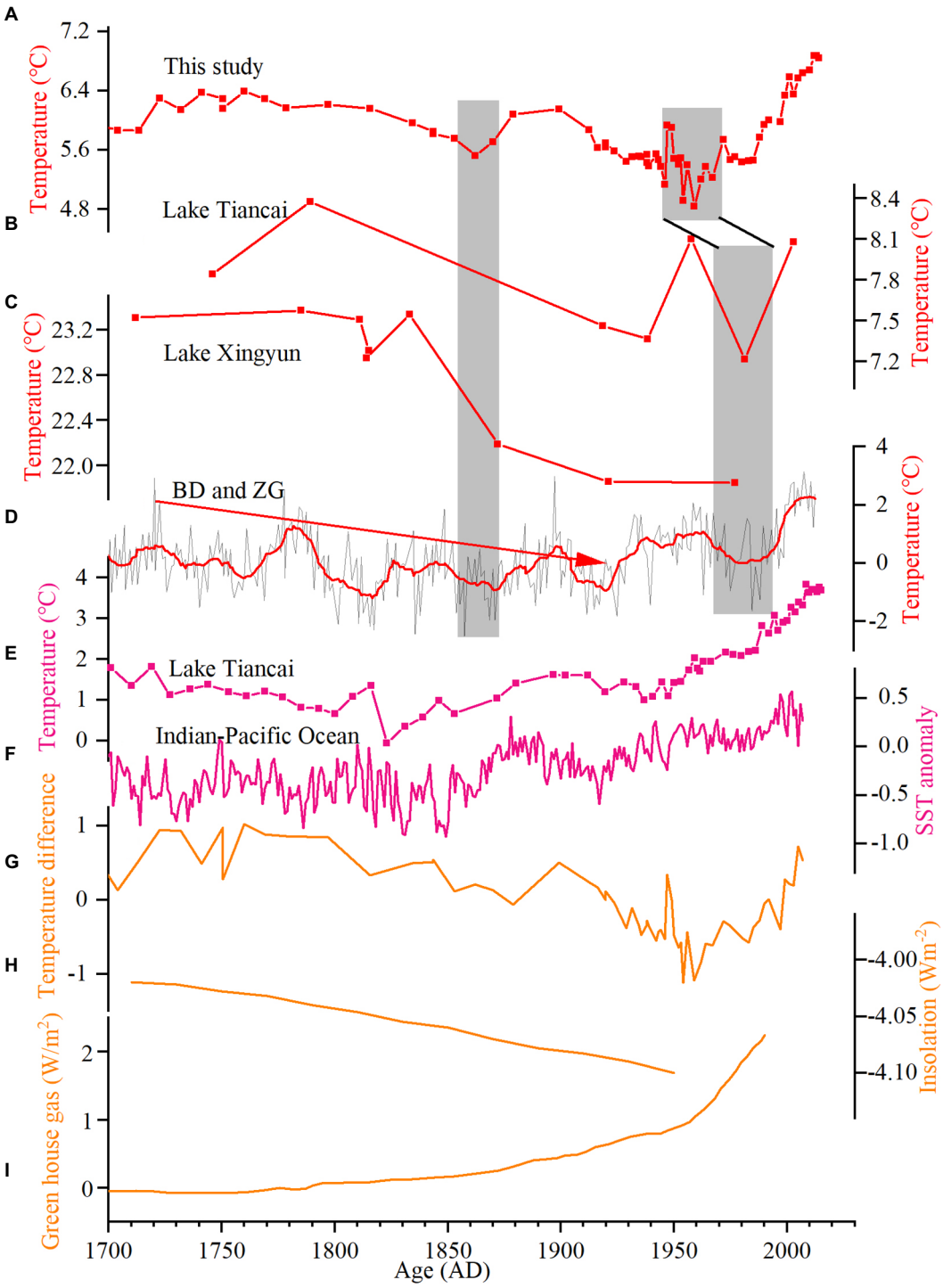

FIGURE 3
Comparison with regional temperature records and driving mechanisms. **(A)** Quantitative temperature reconstruction from Lake Cuoqia in this study. The gray shadows indicate period of low temperature. **(B)** Quantitative mean July temperature reconstruction based on subfossil chironomids from Lake Tiancai (Zhang et al., 2017). **(C)** Pollen-based mean July temperature record from Lake Xingyun (Wu et al., 2018). **(D)** The Apr-Sep mean temperature reconstruction using tree ring from Bangda (BD) and Zuogong (ZG) in the southeastern Tibetan Plateau (Duan and Zhang, 2014). **(E)** Quantitative mean annual air temperature using brGDGTs from Lake Tiancai (Feng et al., 2019). **(F)** The temperature reconstruction of Indian-Pacific Ocean based on coral records (Tierney et al., 2015). **(G)** Temperature difference between our reconstructed temperature anomaly and SST from Indian-Pacific Ocean (Tierney et al., 2015). **(H)** Warm-season insolation anomaly at 26°N (Laskar et al., 2004). **(I)** GHG-driven forcing (Crowley, 2000). (For interpretation of the references to color in this figure legend, the reader is referred to the web version of this article).

An et al., 2014). Furthermore, the pressure difference between Tibetan Plateau and tropical Ocean may also affect the monsoon precipitation and relative humidity in the southeastern Tibetan Plateau (Rashid et al., 2011). Previous studies suggest that the years with high relative humidity are related to the low-pressure conditions on the southeastern Tibetan Plateau, while the pressure field on the Indian Ocean is opposite

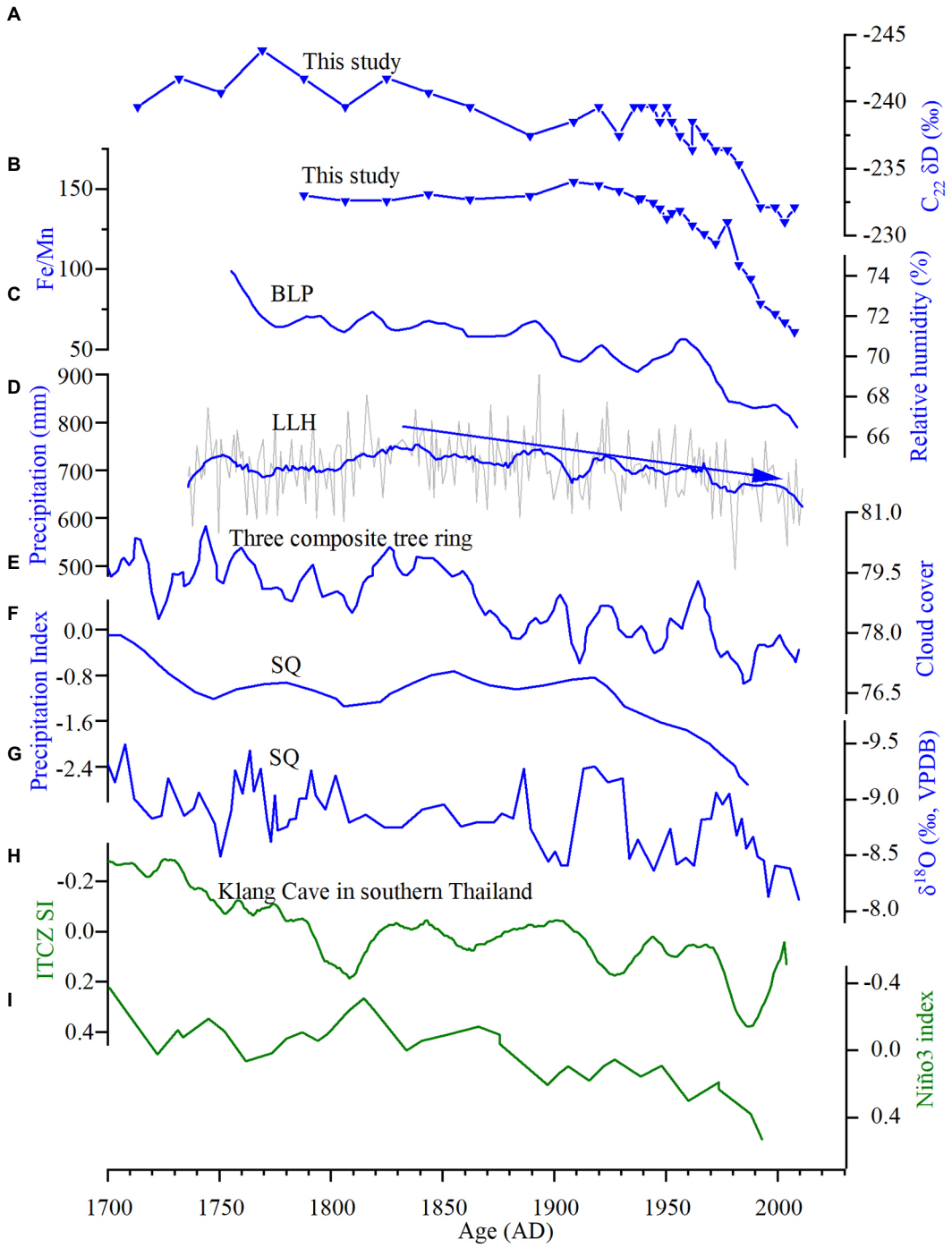

FIGURE 4
Comparison with regional relative humidity records and driving mechanisms. **(A)** δD of C_{22} from fatty acids (this study). **(B)** Changes of lake level inferred from Fe/Mn (this study). **(C)** Reconstructions of relative humidity from June to August based on tree-ring δD chronologies (An et al., 2014). **(D)** Record of $\delta^{18}O$ from regional tree ring (Xu et al., 2019). **(E)** Reconstructed cloud cover using composite $\delta^{18}O$ of three tree-ring chronologies (Liu X. et al., 2014). **(F)** Precipitation index inferred from stalagmite (Tan et al., 2018). **(G)** Stalagmite $\delta^{18}O$ of Shenqi cave (Tan et al., 2018). **(H)** Shift index of Intertropical Convergence Zone inferred from stalagmite (Tan et al., 2019). **(I)** Model simulated Niño3.4 sea surface temperatures variability (Man and Zhou, 2011). (For interpretation of the references to color in this figure legend, the reader is referred to the web version of this article).

(An et al., 2014). When the Tibetan Plateau maintains a high-pressure ridge in summer, the intensity of Indian summer monsoon weakens, reducing the movement of ocean air mass from the Indian Ocean to the plateau (Charles et al., 1997; Xu et al., 2009). Therefore, the path of rain storms will move southward, resulting in low relative humidity. In addition, the decreasing relative humidity over the past 300 years has high coherence with overall southward shift of Intertropical Convergence Zone (Figure 4H; Tan et al., 2019) and intensified EI Niño-like conditions (Figure 4I; Man and Zhou, 2011), indicating a pivotal role of low-latitude driving force to southeastern Tibetan Plateau.

After 1950, our reconstructed temperature record showed consistent changes to the rapid increase in greenhouse gases emission caused by

human activity (Figure 3I), indicating a close connection between them (Crowley, 2000). Although increased temperature can lead to more water-vapor supply and larger temperature difference between sea and land, the relative humidity showed an overall decrease trend during this period (Figure 4A). The decreased relative humidity may be caused by enhanced evaporation associated with unprecedented warming. In addition, the decreasing relative humidity was possibly related to the aerosol-affected Anthropocene warming as well which can lead to a weakening of summer monsoon intensity and thus result into dry environment (Liu et al., 2017). In the future, the continued and rapid warming would further decrease the relative humidity, and more attention should be taken for extreme climate changes in the Tibetan Plateau region.

Conclusion

We reconstruct quantitative warm-season temperature and relative humidity from Lake Cuoqia over the past 300 years, using multiple proxies of brGDGTs, *n*-alkanes, fatty acids and δD of C_{22}. The result of temperature showed decreased trend before 1950 AD and increased trend thereafter, which was consistent with the changes in ACL values of *n*-alkanes and fatty acids in the same core. Our temperature data was also in accord with regional warm-season and/or summer temperature records. The reconstructed relative humidity using C_{22} δD of fatty acids showed gradually dry trend over the past 300 years, which is consistent with the results of lake level inferred from Fn/Mn in the same core and regional $\delta^{18}O$ records from tree ring. Before 1950 AD, temperature and relative humidity were coupled, showing a cold-dry trend. After 1950 AD, the temperature and relative humidity were decoupled, and the temperature began to rise while the relative humidity continued to decline. The temperature is possibly affected by warm-season insolation before 1950 AD. The continuous drying is related to monsoon intensity and water-vapor input caused by the temperature difference between the lake Cuoqia and the Indian-Pacific Ocean. After 1950 AD, the decoupling of temperature and relative humidity may be related to the enhanced evaporation and increased emission of human-induced greenhouse gases and aerosol. The continued and rapid warming would further decrease the relative humidity, and more attention should be taken for extreme climate changes in the Tibetan Plateau region in the future.

Data availability statement

The original contributions presented in the study are included in the article/Supplementary material, further inquiries can be directed to the corresponding author.

Author contributions

TY, CZhang, and HZ designed the conceptualization, conducted data interpretation, drawing and writing. CZhang, HZ, XS, and YL participate in experiments analysis. CZhao, XS, RL, and WZ conducted the research and data interpretation. All authors contributed to the article and approved the submitted version.

Funding

This work was supported by the Jiangsu Special Fund on Technology Innovation of Carbon Dioxide Peaking and Carbon Neutrality (BK20220016), the National Natural Science Foundation of China (42007401), the Strategic Priority Research Program of Chinese Academy of Sciences (XDB40000000), the Laboratory opening project of Liaoning Normal University (#CX202201030), and the Science and Technology Planning Project of NIGLAS (NIGLAS2022TJ02).

Acknowledgments

We thank Yifan Chai, Lingyang Kong, Qian Wang, Xiangdong Yang for field and laboratory assistance.

Conflict of interest

The authors declare that the research was conducted in the absence of any commercial or financial relationships that could be construed as a potential conflict of interest.

Publisher's note

Supplementary material

The Supplementary material for this article can be found online at: https://www.frontiersin.org/articles/10.3389/fevo.2023.1119869/full#supplementary-material

References

An, W., Liu, X., Leavitt, S. W., Xu, G., Zeng, X., Wang, W., et al. (2014). Relative humidity history on the Batang-Litang plateau of western China since 1755 reconstructed from tree-ring $\delta^{18}O$ and δD. *Clim. Dynam.* 42, 2639–2654. doi: 10.1007/s00382-013-1937-z

Appleby, P. G., and Oldfeld, F. (1978). The calculation of lead-210 dates assuming a constant rate of supply of unsupported ^{210}Pb to the sediment. *Catena* 5, 1–8. doi: 10.1016/S0341-8162(78)80002-2

Bansod, S. D., Yin, Z., Lin, Z., and Zhang, X. (2003). Thermal field over Tibetan plateau and Indian summer monsoon rainfall. *Int. J. Climatol.* 23, 1589–1605. doi: 10.1002/joc.953

Cai, Y., Zhang, H., Cheng, H., An, Z., Lawrence Edwards, R., Wang, X., et al. (2012). The Holocene Indian monsoon variability over the southern Tibetan plateau and its teleconnections. *Earth Planet. Sci. Lett.* 335-336, 135–144. doi: 10.1016/j.epsl.2012.04.035

Chai, Y. F., Zhang, C., Kong, L. Y., and Zhao, C. (2018). Climatic changes and heavy metal pollution over the past 200 years recorded by Lake Cuoqia，southwestern Yunnan Province. *J. Lake Sci.* 30, 1732–1744. (in Chinese with English abstract). doi: 10.18307/2018.0624

Charles, C. D., Hunter, D. E., and Fairbanks, R. G. (1997). Interaction between the ENSO and the Asian monsoon in a coral record of tropical climate. *Science* 277, 925–928. doi: 10.1126/science.277.5328.925

Chen, L., Shen, H., Jia, Y., Wu, J., Li, X., Wei, L., et al. (2008). Environmental change inferred from Rb and Sr of lacustrine sediments in Huangqihai Lake, Inner Mongolia. *J. Geogr. Sci.* 18, 373–384. doi: 10.1007/s11442-008-0373-1

Chen, D., Xu, B., Yao, T., Guo, Z., Cui, P., Chen, F., et al. (2015). Assessment of past, present and future environmental changes on the Tibetan Plateau. *Chin. Sci. Bull.* 60, 3025–3035. doi: 10.1360/N972014-01370

Contreras-Rosales, L. A., Jennerjahn, T., Tharammal, T., Meyer, V., Lückge, A., Paul, A., et al. (2014). Evolution of the Indian summer monsoon and terrestrial vegetation in the Bengal region during the past 18 ka. *Quat. Sci. Rev.* 102, 133–148. doi: 10.1016/j.quascirev.2014.08.010

Crowley, T. J. (2000). Causes of climate change over the past 1000 years. *Science* 289, 270–277. doi: 10.1126/science.289.5477.270

Dansgaard, W. (1964). Stable isotopes in precipitation. *Tellus* 16, 436–468. doi: 10.1111/j.2153-3490.1964.tb00181.x

De Jonge, C., Hopmans, E. C., Zell, C. I., Kim, J., Schouten, S., and Sinninghe Damsté, J. S. (2014). Occurrence and abundance of 6-methyl branched glycerol dialkyl glycerol tetraethers in soils: implications for palaeoclimate reconstruction. *Geochim. Cosmochim. Acta* 141, 97–112. doi: 10.1016/j.gca.2014.06.013

Ding, Y. (1992). Effects of the Qinghai-Xizang (Tibetan) plateau on the circulation features over the plateau and its surrounding areas. *Adv. Atmos. Sci.* 9, 112–130. doi: 10.1007/BF02656935

Duan, J., and Zhang, Q. (2014). A 449-year warm season temperature reconstruction in the southeastern Tibetan plateau and its relation to solar activity. *J. Geophys. Res. Atmos.* 119, 11,578–11,592. doi: 10.1002/2014JD022422

Eglinton, T. I., and Eglinton, G. (2008). Molecular proxies for paleoclimatology. *Earth Planet Sc. Lett.* 275, 1–16. doi: 10.1016/j.epsl.2008.07.012

Feng, S., and Hu, Q. (2005). Regulation of Tibetan Plateau heating on variation of Indian summer monsoon in the last two millennia. *Geophys. Res. Lett.* 32:L02702. doi: 10.1029/2004GL021246

Feng, X., Zhao, C., D'Andrea, W. J., Liang, J., Zhou, A., and Shen, J. (2019). Temperature fluctuations during the common era in subtropical southwestern China inferred from brGDGTs in a remote alpine lake. *Earth Planet. Sci. Lett.* 510, 26–36. doi: 10.1016/j.epsl.2018.12.028

Ficken, K. J., Li, B., Swain, D. L., and Eglinton, G. (2000). An n-alkane proxy for the sedimentary input of submerged/floating freshwater aquatic macrophytes. *Org. Geochem.* 31, 745–749. doi: 10.1016/S0146-6380(00)00081-4

He, Y., and Wang, K. (2020). Contrast patterns and trends of lapse rates calculated from near-surface air and land surface temperatures in China from 1961 to 2014. *Sci. Bull.* 65, 1217–1224. doi: 10.1016/j.scib.2020.04.001

Hopmans, E. C., Schouten, S., and Sinninghe Damste, J. S. (2016). The effect of improved chromatography on GDGT-based palaeoproxies. *Org. Geochem.* 93, 1–6. doi: 10.1016/j.orggeochem.2015.12.006

Hou, J., Huang, Y., Wang, Y., Shuman, B., Oswald, W. W., Faison, E., et al. (2006). Postglacial climate reconstruction based on compound-specific D/H ratios of fatty acids from blood pond, New England. *Geochem. Geophys. Geosyst.* 7:1076. doi: 10.1029/2005GC001076

Kaufman, D. S., Ager, T. A., Anderson, N. J., Anderson, P. M., Andrews, J. T., Bartlein, P. J., et al. (2004). Holocene thermal maximum in the western Arctic (0–180°W). *Quat. Sci. Rev.* 23, 529–560. doi: 10.1016/j.quascirev.2003.09.007

Laskar, J., Robutel, P., Joutel, F., Gastineau, M., Correia, A. C. M., and Levrard, B. (2004). A long-term numerical solution for the insolation quantities of the earth. *Astron. Astrophys.* 428, 261–285. doi: 10.1051/0004-6361:20041335

Liu, J., Chen, J., Selvaraj, K., Xu, Q., Wang, Z., and Chen, F. (2014). Chemical weathering over the last 1200 years recorded in the sediments of Gonghai Lake, Lvliang Mountains, North China: a high-resolution proxy of past climate. *Boreas* 43, 914–923. doi: 10.1111/bor.12072

Liu, H., and Liu, W. (2019). Hydrogen isotope fractionation variations of n-alkanes and fatty acids in algae and submerged plants from Tibetan plateau lakes: implications for palaeoclimatic reconstruction. *Sci. Total Environ.* 695:133925. doi: 10.1016/j.scitotenv.2019.133925

Liu, J., Rühland, K. M., Chen, J., Xu, Y., Chen, S., Chen, Q., et al. (2017). Aerosol-weakened summer monsoons decrease lake fertilization on the Chinese loess plateau. *Nat. Clim. Chang.* 7, 190–194. doi: 10.1038/nclimate3220

Liu, X., Xu, G., Grießinger, J., An, W., Wang, W., Zeng, X., et al. (2014). A shift in cloud cover over the southeastern Tibetan plateau since 1600: evidence from regional tree-ring d18O and its linkages to tropical oceans. *Quat. Sci. Rev.* 88, 55–68. doi: 10.1016/j.quascirev.2014.01.009

Mackereth, F. J. H. (1966). Some chemical observations on post-glacial lake sediments. *Phil. Trans. R. Soc. Lond. B* 250, 165–213. doi: 10.1098/rstb.1966.0001

Man, W., and Zhou, T. (2011). Forced response of atmospheric oscillations during the last millennium simulated by a climate system model. *Chin. Sci. Bull.* 56, 3042–3052. doi: 10.1007/s11434-011-4637-2

Meyers, P. A., and Ishiwatari, R. (1993). Lacustrine organic geochemistry-an overview of indicators of organic matter sources and diagenesis in lake sediments. *Org. Geochem.* 20, 867–900. doi: 10.1016/0146-6380(93)90100-P

Peterse, F., Prins, M. A., Beets, C. J., Troelstra, S. R., Zheng, H., Gu, Z., et al. (2011). Decoupled warming and monsoon precipitation in East Asia over the last deglaciation. *Earth Planet. Sci. Lett.* 301, 256–264. doi: 10.1016/j.epsl.2010.11.010

Rashid, H., England, E., Thompson, L., and Polyak, L. (2011). Late glacial to Holocene Indian summer monsoon variability based upon sediment records taken from the bay of Bengal. *Terr. Atmos. Ocean. Sci.* 22, 215–228. doi: 10.3319/TAO.2010.09.17.02(TibXS)

Russell, J. M., Hopmans, E. C., Loomis, S. E., Liang, J., and Sinninghe Damsté, J. S. (2018). Distributions of 5- and 6-methyl branched glycerol dialkyl glycerol tetraethers (brGDGTs) in east African lake sediment: effects of temperature, pH, and new lacustrine paleotemperature calibrations. *Org. Geochem.* 117, 56–69. doi: 10.1016/j.orggeochem.2017.12.003

Sachse, D., Billault, I., Bowen, G. J., Chikaraishi, Y., Dawson, T. E., Feakins, S. J., et al. (2012). Molecular Paleohydrology: interpreting the hydrogen-isotopic composition of lipid biomarkers from photosynthesizing organisms. *Annu. Rev. Earth Planet. Sci.* 40, 221–249. doi: 10.1146/annurev-earth-042711-105535

Sachse, D., Radke, J., and Gleixner, G. (2004). Hydrogen isotope ratios of recent lacustrine sedimentary n-alkanes record modern climate variability. *Geochim. Cosmochim. Acta* 68, 4877–4889. doi: 10.1016/j.gca.2004.06.004

Schouten, S., Hopmans, E. C., and Sinninghe Damsté, J. S. (2013). The organic geochemistry of glycerol dialkyl glycerol tetraether lipids: a review. *Org. Geochem.* 54, 19–61. doi: 10.1016/j.orggeochem.2012.09.006

Shen, J., Xue, B., Wu, J. L., Wu, Y. H., Liu, X. Q., Yang, X. D., et al. (2010). *Lake Sedimentation and Environmental Evolution*. Beijing: Science Press.

Sinninghe Damste, J. S., Ossebaar, J., Abbas, B., Schouten, S., and Verschuren, D. (2009). Fluxes and distribution of tetraether lipids in an equatorial African lake: constraints on the application of the TEX_{86} palaeothermometer and BIT index in lacustrine settings. *Geochim. Cosmochim. Acta* 73, 4232–4249. doi: 10.1016/j.gca.2009.04.022

Sun, Q., Chu, G., Liu, M., Xie, M., Li, S., Ling, Y., et al. (2011). Distributions and temperature dependence of branched glycerol dialkyl glycerol tetraethers in recent lacustrine sediments from China and Nepal. *J. Geophys. Res. Biogeosci.* 116:1365. doi: 10.1029/2010JG001365

Sun, X., Zhao, C., Zhang, C., Feng, X., Yan, T., Yang, X., et al. (2021). Seasonality in Holocene temperature reconstructions in southwestern China. *Paleoceanogr. Paleoclimatol.* 36:e2020PA004025. doi: 10.1029/2020PA004025

Tan, L., Cai, Y., Cheng, H., Edwards, L. R., Lan, J., Zhang, H., et al. (2018). High resolution monsoon precipitation changes on southeastern Tibetan plateau over the past 2300 years. *Quat. Sci. Rev.* 195, 122–132. doi: 10.1016/j.quascirev.2018.07.021

Tan, L., Shen, C., Löwemark, L., Chawchai, S., Edwards, R. L., Cai, Y., et al. (2019). Rainfall variations in central indo-Pacific over the past 2,700 y. *P. Natl. Acad. Sci. U.S.A.* 116, 17201–17206. doi: 10.1073/pnas.1903167116

Tierney, J. E., Abram, N. J., Anchukaitis, K. J., Evans, M. N., Giry, C., Kilbourne, K. H., et al. (2015). Tropical Sea surface temperatures for the past four centuries reconstructed from coral archives. *Paleocean* 30, 226–252. doi: 10.1002/2014PA002717

Wu, D., Chen, X., Lv, F., Brenner, M., Curtis, J., Zhou, A., et al. (2018). Decoupled early Holocene summer temperature and monsoon precipitation in Southwest China. *Quat. Sci. Rev.* 193, 54–67. doi: 10.1016/j.quascirev.2018.05.038

Xiao, X., Haberleb, S. G., Shen, J., Yang, X., Han, Y., Zhang, E., et al. (2014). Latest Pleistocene and Holocene vegetation and climate history inferred from an alpine lacustrine record, northwestern Yunnan Province, southwestern China. *Quat. Sci. Rev.* 86, 35–48. doi: 10.1016/j.quascirev.2013.12.023

Xu, C., An, W., Wang, S. Y. S., Yi, L., Ge, J., Nakatsuka, T., et al. (2019). Increased drought events in Southwest China revealed by tree ring oxygen isotopes and potential role of Indian Ocean dipole. *Sci. Total Environ.* 661, 645–653. doi: 10.1016/j.scitotenv.2019.01.186

Xu, H., Hong, Y. T., Hong, B., Zhu, Y. X., and Wang, Y. (2009). Influence of ENSO on multi-annual temperature variations at Hongyuan, NE Qinghai-Tibet plateau: evidence from d13C of spruce tree rings. *Int. J. Climatol.* 30, 120–126. doi: 10.1002/joc.1877

Xu, C., Sano, M., Dimri, A. P., Ramesh, R., Nakatsuka, T., Shi, F., et al. (2018). Decreasing Indian summer monsoon on the northern Indian sub-continent during the last 180 years: evidence from five tree-ring cellulose oxygen isotope chronologies. *Clim. Past* 14, 653–664. doi: 10.5194/cp-14-653-2018

Yan, T., Zhao, C., Yan, H., Shi, G., Sun, X., Zhang, C., et al. (2021). Elevational differences in Holocene thermal maximum revealed by quantitative temperature reconstructions at ~30° N on eastern Tibetan plateau. *Palaeogeo. Palaeoclim. Palaeoec.* 570:110364. doi: 10.1016/j.palaeo.2021.110364

Yang, H., and Huang, Y. (2003). Preservation of lipid hydrogen isotope ratios in Miocene lacustrine sediments and plant fossils at clarkia, northern Idaho, USA. *Org. Geochem.* 34, 413–423. doi: 10.1016/S0146-6380(02)00212-7

Yao, T., Xue, Y., Chen, D., Chen, F., Thompson, L. G., Cui, P., et al. (2019). Recent third Pole's rapid warming accompanies cryospheric melt and water cycle intensification and interactions between monsoon and environment: multidisciplinary approach with observations, modeling, and analysis. *Bull. Am. Meteorol. Soc.* 100, 423–444. doi: 10.1175/BAMS-D-17-0057.1

Zhang, E., Chang, J., Cao, Y., Sun, W., Shulmeister, J., Tang, H., et al. (2017). Holocene high-resolution quantitative summer temperature reconstruction based on subfossil chironomids from the southeast margin of the Qinghai-Tibetan plateau. *Quat. Sci. Rev.* 165, 1–12. doi: 10.1016/j.quascirev.2017.04.008

Zhang, W., Liu, B. B., Li, Y. H., Feng, J., Zhang, B., Wang, Z. L., et al. (2012). Quaternary glacier development and environmental evolution in Qianhu Mountain, North-Western Yunnan Province. *Acta Geogra. Sinica* 67, 657–670. doi: 10.11821/xb201205008

Zhang, C., Zhao, C., Yu, S., Yang, X., Cheng, J., Zhang, X., et al. (2022). Seasonal imprint of Holocene temperature reconstruction on the Tibetan plateau. *Earth-Sci. Rev.* 226:103927. doi: 10.1016/j.earscirev.2022.103927

Zhang, C., Zhao, C., Yu, Z., Zhang, H., Zhou, A., Zhang, X., et al. (2020). Western Pacific Ocean influences on monsoon precipitation in the southwestern Chinese loess plateau since the mid-Holocene. *Clim. Dyn.* 54, 3121–3134. doi: 10.1007/s00382-020-05159-9

Zhang, C., Zhao, C., Zhou, A., Zhang, K., Wang, R., and Shen, J. (2019). Late Holocene lacustrine environmental and ecological changes caused by anthropogenic activities in the Chinese loess plateau. *Quat. Sci. Rev.* 203, 266–277. doi: 10.1016/j.quascirev.2018.11.020

Zhao, C., Cheng, J., Wang, J., Yan, H., Leng, C., Zhang, C., et al. (2021b). Paleoclimate significance of reconstructed rainfall isotope changes in Asian monsoon region. *Geophy. Res. Lett.* 48:e92460. doi: 10.1029/2021GL092460

Zhao, C., Rohling, E. J., Liu, Z., Yang, X., Zhang, E., Cheng, J., et al. (2021a). Possible obliquity-forced warmth in southern Asia during the last glacial stage. *Sci. Bull.* 66, 1136–1145. doi: 10.1016/j.scib.2020.11.016

Zhou, W., Xie, S., Meyers, P. A., and Zheng, Y. (2005). Reconstruction of late glacial and Holocene climate evolution in southern China from geolipids and pollen in the Dingnan peat sequence. *Org. Geochem.* 36, 1272–1284. doi: 10.1016/j.orggeochem.2005.04.005